VIII International Conference on Particle-Based Methods
PARTICLES 2023
U. Perego, M. Cremonesi, A. Franci (Eds)

FAILURE OF COHESIVE GRANULAR COLUMNS: FRICTION AND CONTACT ADHESION

L. STARON[1], L. DUCHEMIN[2] AND P.-Y. LAGREE[1]

[1]Institut d'Alembert,
CNRS - Sorbonne Université - UMR 7190
Paris 75252 Cedex 5, France

[2] Physique et Mécanique des Matériaux Hétérogènes
ESPCI Paris - UMR 7636
75252 Paris Cedex 5, France

Abstract: This contribution focuses on the influence of the existence of a debonding length onto the behaviour of a cohesive granular sample. We apply a contact dynamics algorithm to study the effect of both contact adhesion strength and debonding length on the failure of a cohesive step, analysing a set of independent simulations. Contact adhesion strength coincides with stronger pile stability and larger apparent friction in the absence of any debonding length. We show that the existence of a larger debonding length amplifies this phenomenology. At large adhesion strength, we observe the existence of a sharp modification of the behaviour of the system even in the case of a very small debounding length, compared to the case of the absence of the latter.
We compare the performance of the algorithm in the different cases, and show how increasing the debonding length leads to a better precision of the hard-core approximation.

Keywords. Contact Dynamics, Cohesive failure, Debonding length, Friction

1 INTRODUCTION

Cohesive granular materials are omnipresent in manufacturing techniques, where they are the source of many difficulties. As a consequence, significant work has been carried out to describe the range of behaviour of cohesive material and characterise the corresponding properties [1, 2, 3]. Academic considerations have also prompted numerous works, leading to both theoretical and experimental advances [4, 5, 6, 7, 8]. The need for measurable well-constrained quantities often implies the use of wet granular matter, where cohesion is induced by capillary bridges [5, 6]. A recent alternative involves sticky polymeric coatings, which allow for quantitative measurements at both low and high contact adhesion, without the existence of capillary structures [7].

An important difference between these two experimental cohesive materials lies in the nature of the adhesive interaction creating the cohesive bonds. Wet contacts involve a cohesion depending on the stretching of a meniscus; the maximum stretching allowed before the contact is lost defines the debonding (or rupture) distance. By contrast, sticky

coatings imply a short-range cohesive interaction: contacts are lost as soon as the two contacting grains move away one from another. In this contribution, we are interested in quantifying the influence of the existence of a debonding length onto the behaviour of a cohesive granular sample, including its stability, and its internal coefficient of friction.

Numerical simulations are a powerfull tool to examine the complexity of cohesive behaviour [9, 10]. Here we apply a Contact Dynamics algorithm to study the effect of both contact adhesion strength and debonding length on the behaviour of the simulated systems. Many works addressing the behaviour of cohesive granular matter adopt a stationary, uniform flow configuration. By contrast, the configuration adopted in this study, namely the gravity-driven failure of cohesive columns, implies neither a uniform nor a stationary flow. Analysing a minimal set of 35 independent simulations, we investigate how the existence of a debonding length changes the influence of the contact adhesion intensity. We first study how contact adhesion strength coincides with stronger pile stability and larger apparent friction in the absence of any debonding length. We then study how the existence of a larger debonding length significantly stabilizes the system, and increases the internal friction, in agreement with both experimental and numerical studies of homogeneous shear flows [5, 6]. At large adhesion strength, we observe the existence of a sharp modification of the behaviour of the system even in the case of a very small debounding length, compared to the case of the absence of the latter.
Finally, we compare the performance of the algorithm in the different cases. We show how increasing the debonding length leads to smaller overlap at contacts, improving the precision of the hard-core hypothesis, fundamental in the algorithm.

2 THE NUMERICAL EXPERIMENT

2.1 The Contact Dynamics algorithm

A Contact Dynamics algorithm is applied to simulate two-dimensional (2D) cohesive systems [11]. The grains are perfectly rigid circular beads with a diameter randomly chosen in the interval $[4.10^{-3}\text{m}; 6.10^{-3}\text{m}]$, and a mean diameter $d = 5.10^{-3}\text{m}$, to prevent crystalline ordering. Each contact is made cohesive through the introduction of a negative (*i.e.* tensile) force threshold $-F_c$ in the Signorini's contact graph, which specifies the acceptable values for the contact normal force N, compatible with the unilateral condition imposed by the grains rigidity (see [11] for details). An Amontons-Coulomb friction law is implemented, involving the contact coefficient of friction μ_c. The tangential force threshold is supplemented with the adhesive force threshold: sliding is permitted when the tangential force has reached $\mu_c(N + F_c)$. The microscopic coefficient of friction is not varied: $\mu_c = 0.2$. The grains also interact through inelastic collisions, with a coefficient of restitution set to zero. Their volumetric density is $\rho = 0.1\,\text{kg.m}^{-2}$.
A comprehensive presentation of the CD method will be found in Radjai & Richefeu [11]. The adhesive force threshold F_c is given in number of grains mean weight through the

introduction of a granular Bond number B_{og} [12, 9]:

$$F_c = B_{og}\, m\, g, \tag{1}$$

where m is the mean mass of the two grains in contact. The granular Bond number thus quantifies the contact adhesion compared to the grains weight. It also sets the value of the macroscopic cohesive stress of the systems, although relating the latter to the contact adhesion is not straightforward [13, 4, 14].

The system state is recorded every $\Delta t = 10^{-3}$s. The computational time step is set to $dt = 2.10^{-4}$s.

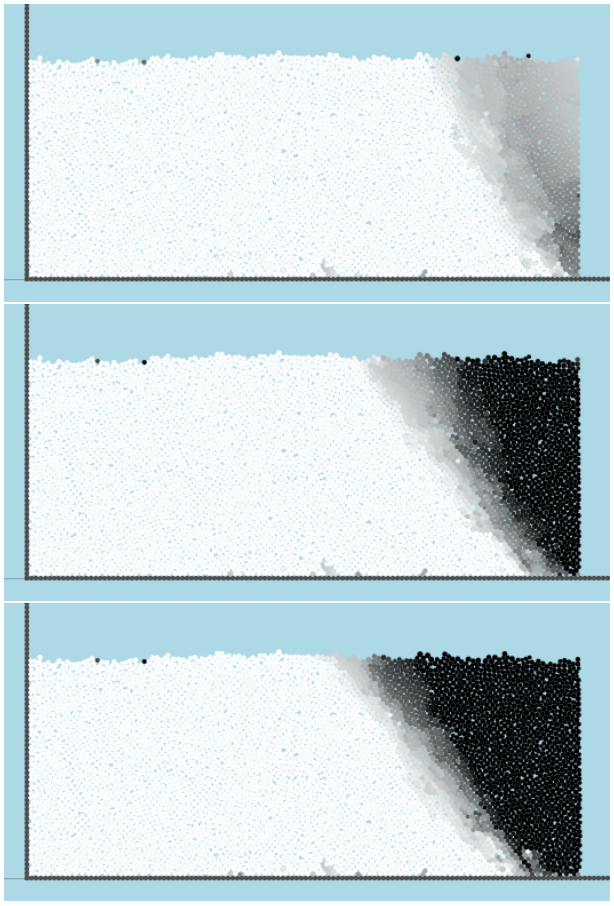

Figure 1: Granular sample with a contact adhesion B_{og}= 30, at instant t/T = 0.10, 0.14, and 0.18 from top to bottom ($T = \sqrt{H/g}$). The gray colorscale shows the cumulative displacement of the grains between $0.10d$ (white bounding shade) and $0.15d$ (black bounding shade).

2.2 Generation of initial states

The systems are generated by deposition under gravity of 5970 circular grains in a rectangular container. The grains are initially cohesionless, and the contacts involve a

weak contact friction $\mu_c = 0.2$. Consequently, the grains rest and relaxe forming a dense packing with a volume fraction $\phi \simeq 0.82$. When the systems have reached equilibrium, and all the grains are at rest, a large adhesive contact force is applied in order to sinter the structure.

The systems are bounded on the left hand side by a rigid vertical wall (Figure 1). The columns have an initial height $H \simeq 49d$ and a width $R \simeq 120d$, namely an aspect ratio $a \simeq 0.41$. This squat geometry allows for the generation of failures far enough from the left wall so that they remain unaffected by its presence.

When launching the collapse simulation, the right wall closing the container is removed, and the granular Bond number, namely the contact adhesion strength, is set to the desired value.

2.3 Unfolding of a failure

At initial time $t = 0$, the right-hand-side wall is removed, and the columns are left to fail onto a horizontal plane made rough by gluing grains on it (Figure 1). Because the present work is interested in the failure onset, and not on the ensuing spreading, we focus on the first instants of the evolution, namely $t < 0.19T$, with $T = \sqrt{H/g} \simeq 0.158s$.

The granular Bond number is successively set to B_{og}= 5, 10, 20, 30, 40, and 60. In addition, the non-cohesive case B_{og}= 0 is also considered.

The column height $H \simeq 49d$ of the system, and the combination of contact adhesion explored, coincide with unstable states as studied in Abramian et al 2020 for similar systems [16]. If we suppose that the yielding height H_y satisfies $H_y/d \simeq 0.5B_{ond}$, as observed in [16], the systems studied here range from $H/H_y \simeq 1.6$ for B_{og}= 60, to $H/H_y \simeq 10$ for B_{og}= 10. For smaller B_{og} numbers, the predicted yielding height is smaller than $5d$. In that finite-size limit, the definition of a yielding height itself, according to a continuum picture of the systems, is no longer straightforward.

As the system is left to evolve under gravity unchecked by the right-hand-side wall, no noticeable motion of the grains is observed, as can be infered from Figure 1. However, the packings do evolve and grains rearrange depending on the value of the contact adhesion. Figure 1 shows the cumulative displacement of the grains in a $[0.1d, 0.15d]$ range for a contact adhesion B_{og}= 30: we clearly see the emergence of a failing block. The ensuing motion and failure/deposit characteristic are more specifically addressed in [15, 14]. In this contribution, we rather focus on the quasi-static evolution characterizing the failure onset, namely for $t/T < 0.19$ ($T = \sqrt{H/g}$). Over this time interval, the mean velocity of the grains is very small, as can be seen in Figure 2, even in the case of a cohesionless system (B_{og}= 0), for which the mean grain velocity remains lower than $0.2\sqrt{gd}$.

In the following, we compute the stress tensor in the whole simulation time span $t/T \in [0 : 0.19]$, and derive the value of the effective coefficient of friction μ^*. Then, we test the effect of introducing a debonding length in the contact model, thereby taking into

account the existence of an hysteresis in the adhesive behaviour: cohesive contacts forms and open at different grains distance. We can then study how the value of this debonding length affects the behaviour of the granular samples.

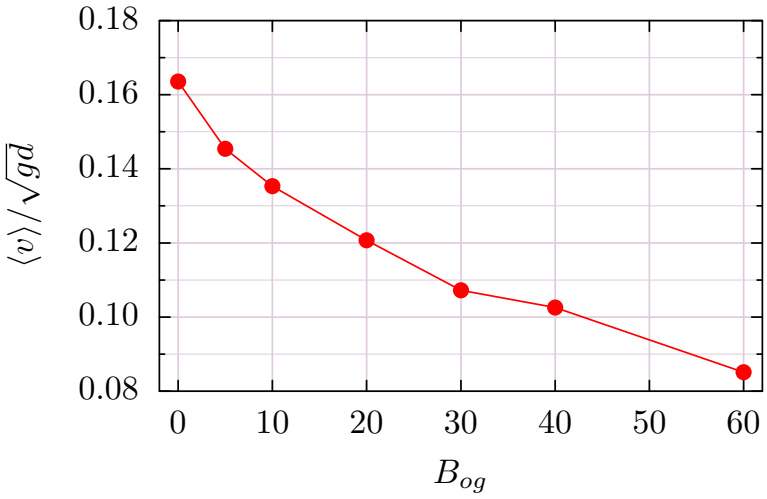

Figure 2: Mean velocity of the grains in the whole simulation time interval $t \in [0 : 0.19T]$, normalised by $\sqrt{gd}$, as a function of the contact adhesion B_{og}.

3 CONTACT ADHESION AND APPARENT FRICTION

3.1 The stress tensor

Stresses are computed following the classical micro-mechanical definition, considering forces transmitted by long-lasting contact interactions, and by short-lived collisions induced by velocity fluctuations [5]. These two contributions, quantified by the static stress tensor σ^s and the kinetic stress tensor σ^k, form the total stress tensor σ:

$$\begin{aligned} \sigma &= \sigma^s + \sigma^k, \\ \sigma &= \frac{1}{V} \sum_{c \in N_c} \mathbf{f}^c \otimes \mathbf{r}^c + \frac{1}{V} \sum_{p \in N_p} m_p \delta \mathbf{v}^p \otimes \delta \mathbf{v}^p, \end{aligned}$$

where $\mathbf{f}^c$ is the force transmitted by the contact c and $\mathbf{r}^c$ is the center-to-center vector, m_p is the mass of the grain p, $\delta \mathbf{v}^p$ its velocity fluctuations, N_c and N_p are the number of contacts and grains respectively over which the summation is made, V is the volume over which the stress is computed, and $\otimes$ is the dyadic product.
The volume V of the samples is considered to be constant and equal to its value in the initial state. The volumes variations over the duration of the simulations being less than 0.5% for all samples, this approximation is acceptable.
The ratio of the static pressure P^s to the total pressure P, computed respectively from the

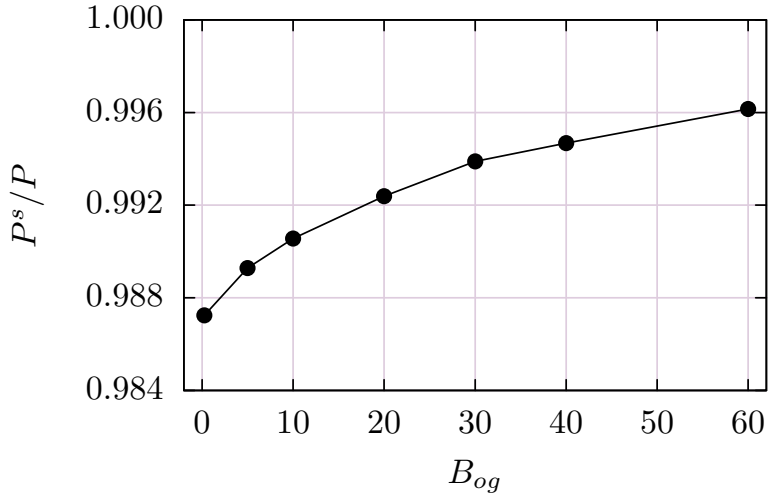

Figure 3: Ratio of the pressure P^s measured by the static stress tensor $\sigma^{\mathbf{s}}$ to the total pressure P measured by the total stress tensor σ, evaluated over the duration of the simulations, as a function of the granular Bond number B_{og}. The static stress tensor is consistently dominating the total stress, denoting a quasi-static, or very slow evolution ($P^s/P > 98\%$). We observe that strong adhesive forces favour the contribution of the static tensor, with the ratio P^s/P increasing with B_{og} .

static stress tensor σ^s and total stress tensor σ, is plotted in Figure 3 as a function of the granular Bond number B_{og}. The large values exhibited by P^s/P, above 0.98 for all B_{og}, bespeak a stress state largely dominated by the contact network: kinetic contributions are negligeable. This is consistent with the very small volume variations. Moreover, we observe how adhesion favours the contribution of the static stress to the total stress state, with P^s/P increasing with B_{og}.

In the following, we will consider the whole simulations time interval to evaluate the apparent friction associated to the failure onset.

3.2 The apparent friction μ^*

The apparent friction μ^* is defined as the ratio of the deviatoric stress Q to the pressure P, both computed as functions of the eigenvalues of the total stress tensor σ: $\mu^* = Q/P$, with $P = (\lambda_1 + \lambda_2)/2$ and $Q = (\lambda_1 - \lambda_2)/2$.
Figure 4 shows the apparent friction μ^* measured and/or computed for sheared samples of wet granular matter as a function of the reduced pressure P^* in Khamseh et al 2015 [5] and in Badetti et al 2018 [6] (see [1] for details). The reduced pressure is defined as the ratio of the system characteristic pressure (or normal confining stress) and the characteristic adhesive stress, namely comparing the cohesion with the mean stress level of the system [5, 6]. In the simulations discussed here, presenting unconfined failures, the only pressure stems from gravity. We thus define the reduced pressure P^* as the

[1] Data extracted from Table 1 in [5], and from Figure 7 in [6]

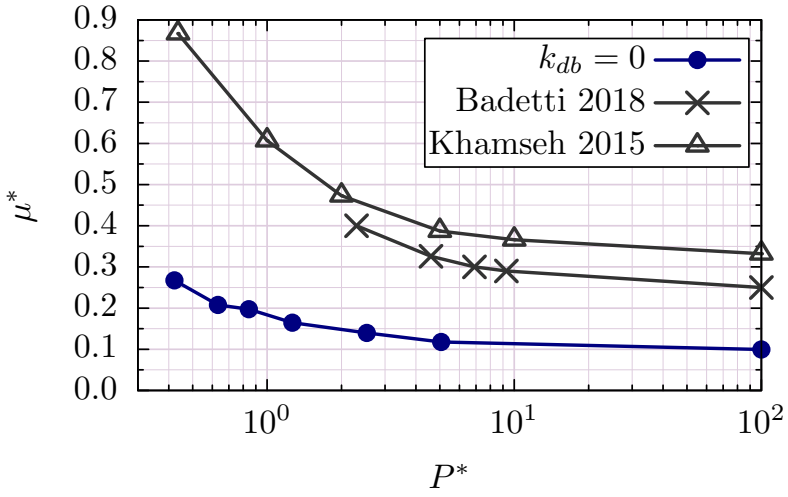

Figure 4: Apparent friction μ^* computed in the failure over the whole simulation as a function of the reduced pressure P^*. The data from [5, 6] are also reproduced.

ratio of the gravity-induced pressure seen by the centre of mass of the packing $\frac{1}{2}\rho\phi gH$ (where ϕ is the solid fraction) divided by the contact adhesive stress F_c/d, thus giving $P^* = (2\phi H)/(\pi d B_{og}) \simeq 25.3/B_{og}$.

The simulations apparent friction μ^* is displayed in Figure 4 together with the data from [5, 6]. Note that we have artificially defined $P^* = 100$ for $B_{og} = 0$, in order to allow for comparison with the very low cohesion data from [5, 6]. The behaviours are very comparable in terms of dependence on P^*, exhibiting a marked increase with $1/P^*$. However, the values of μ^* of the simulations are much weaker, with $\mu^* \simeq 0.1$ for $P^* \to \infty$ and $\mu^* \simeq 0.27$ for $P^* \to 0$, instead of 0.33 and 0.87 observed by [5] for instance.

A first element to explain this discrepancy could be that the simulated samples are unconfined. While the packings are yielding as a result of gravity, no walls do oppose the onset of the collapse dynamics, and no external forcing permits the stress state to build up.

An other source of descripency lies in the contact model implemented to simulate cohesive matter. Indeed, beside the differences between implicit CD and explicit DEM methods inherent to the algorithms, [5, 6] are considering wet systems, where adhesive forces are capillary bridges. An essential feature of this type of adhesive interactions is the existence of a debonding (or rupture) distance, beyond which the contacts do open and the attractive forces vanish. The existence and extension of this debonding distance was shown to play a significant role in the value of the apparent friction [5]. By contrast, our cohesive samples are simple sticky beads, with short-ranged adhesion, for which attractive forces vanish as soon as contacting grains part.

In the following, we will examine how the implementation of a debonding length in the contact model affects the frictional properties and the behaviour of the failing steps.

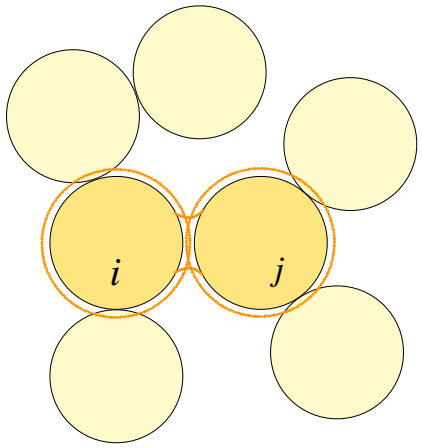

Figure 5: Debonding length: where a cohesive contact is opening, the grains diameter is locally increased in order to keep the opening contact in a grain-touching state, thus mimicking the formation of a capillary bond.

4 EFFECT OF IMPLEMENTING A DEBONDING LENGTH

4.1 Implementation

A cohesive contact may form ar soon as two grains touch, namely as soon as the distance between their centres of mass equals the sum of their diameters. However, the breaking up of the contact may require a different condition. The cohesive interaction may vanish only when the gap between the two contacting grains increases beyond a given value, not limited by their respective diameter. This value defines the debonding length. In a wet granular media for instance, this length coincides with the maximum extension of a capillary bond.

In our simulations, the grains are circular beads with a given diameter d. To define a debonding length, we need to identify the cohesive contacts which would open if their diameter was left unchanged. But because contacts are very local, the modifications needed to preserve an opening contact are also local. We just consider locally an *effective* grains radius, which, its value being larger than that of the initial radius, will lead to the detection, hence the resolution, of the opening contact. This strategy is illustrated in Figure 5.

Practically, we introduce a debonding factor k_{db}. If r_i is the radius of a grain i, involved in a cohesive contact with the grain j, then the opening of the contact will lead to a local increase of both radius, forming the effective radius r'_i and r'_j:

$$r'_i = r_i\,(1 + k_{db}) \quad \text{and} \quad r'_j = r_j\,(1 + k_{db}).$$

Thereby, the gap opening between the two grains is "effectively" reduced. While the distance between the two centres of mass exceeds the sum of their real radius, it will nev-

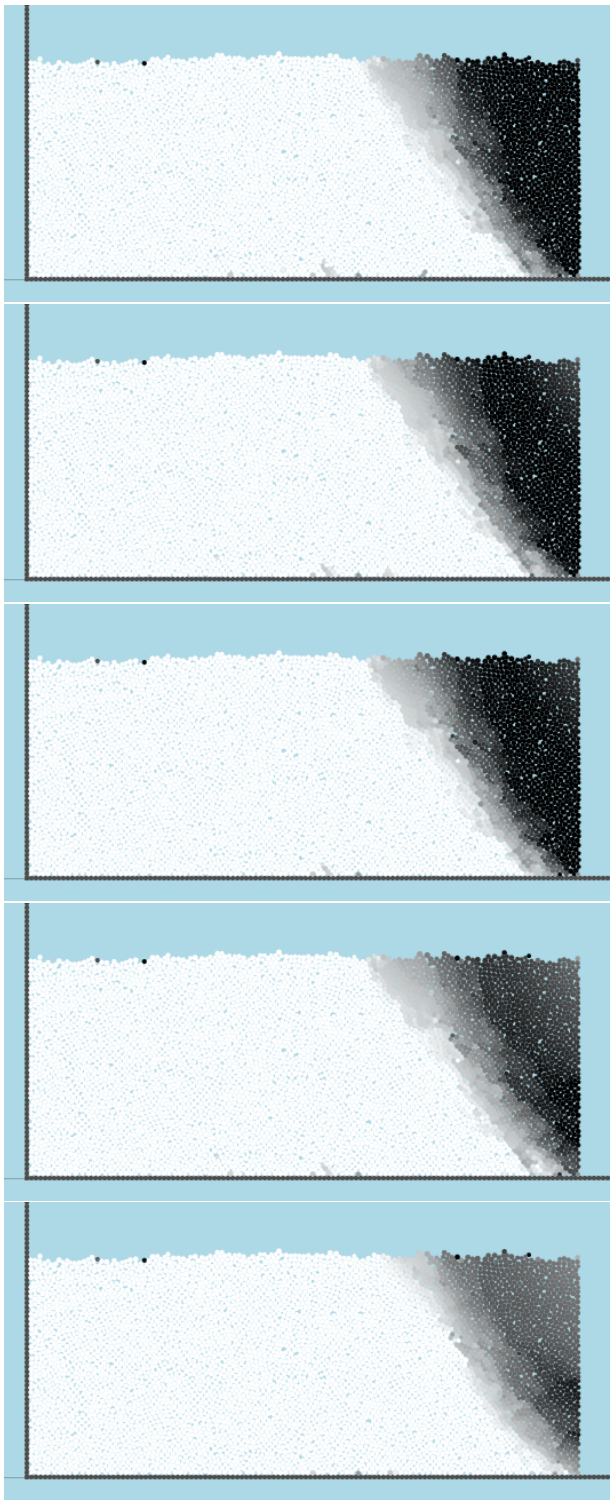

Figure 6: Granular sample with a contact adhesion B_{og}= 30, at instant $t/T = 0.14$, for different values of the debonding length: from top to bottom, $k_{db} = 0$, 5.10^{-4}, 1.10^{-3}, 2.10^{-2}, and 1.10^{-1}. The gray colorscale shows the cumulative displacement of the grains between $0.10d$ (white bounding shade) and $0.15d$ (black bounding shade).

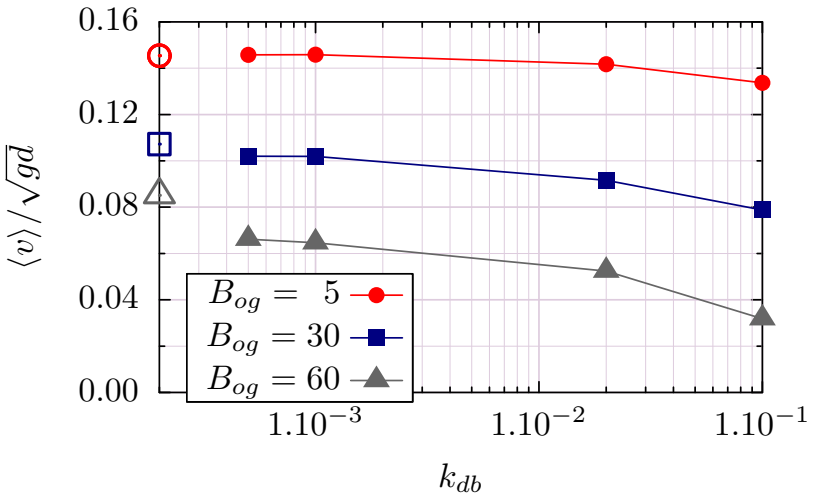

Figure 7: Mean velocity of the grains over the simulation interval ($t \in [0, 0.19T]$) as a function of the debonding factor k_{db}. Three values of the contact adhesion are shown: $B_{og} = 5$, 30 and 60; the empty symbols stand for the case $k_{db} = 0$.

ertheless lead to the detection of a contact as long as this distance remains lower than the sum of their effective radius. The extra length given by $k_{db}(r_i + r_j)$ forms the debonding length ℓ_{db}.

In the lab, the existence of a debonding distance is usually related to the existence of a capillary bridge in humid/wet granular matter. When two grains forming a cohesive contact start separating, the cohesive force will endure as long as the meniscus volume is sufficient for the cohesive bond to stretch without breaking. The cohesive properties of a wet granular media is thus related to the volume of liquid added to the sample. From Khamseh et al 2015 [5], the debonding length in a wet granular media varies from $\ell_{db}/d = 10^{-2}$ to $\ell_{db}/d = 10^{-1}$.

No such capillary structure is observed in cohesive media designed with a controlled polymeric coating such as in Gans et al 2020 [7]. In that case, the presence of a debonding length cannot be asserted. Yet if its existence was to be postulated, a good estimation of its extent would be given by the thickness of the cohesive coating. From [7], $\ell_{db}/d = 5.10^{-4}$ is a reasonable option.

In the following, we thus probe the effect of the existence of a debonding lenth by setting alternatively the debonding factor $k_{db} = \ell_{db}/d$ to very small to large values, consistently with the experimental observation, namely $k_{db} = 5.10^{-4}$, 1.10^{-3}, 2.10^{-2} and 1.10^{-1}. The case $k_{db} = 0$ is also systematically discussed in the light of the results.

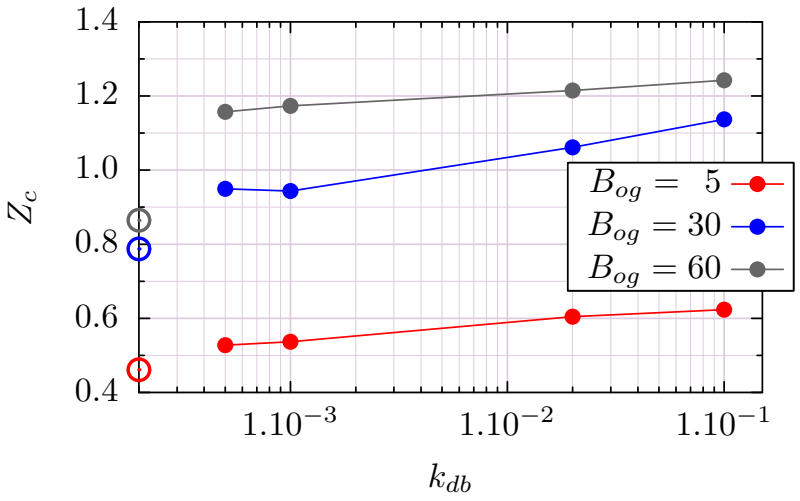

Figure 8: Density of cohesive contacts Z_c as a function of the debonding factor k_{db} for three values of the contact adhesion B_{og}=5, 30 and 60.

4.2 Increasing the effective cohesion

An immediate consequence of the existence of a debonding length is to change the mean cohesive properties of the granular material. This effect would be best evidenced by estimating the cohesive stress τ_c of the systems. However, such an estimation is far from being straightforward [13, 4]. This is particularly true for transient inhomogeneous evolution, like the onset of a gravity driven failure studied here.

However, the effect of the debonding length can be infered from the dynamics of the systems. Plotting the mean velocity of the grains averaged over the whole simulation time interval (Figure 7) shows clearly that, for a given value of the contact adhesion, larger debonding lengths coincide with smaller velocities. This effect is more pregnant for stronger adhesion, eg $B_{og} = 60$. The cases coinciding with $k_{db} = 0$ are also shown in the same graph for comparison (the corresponding points are arbitrarily plotted on the y axis, the absisse not being compatible with the logarithmic scale of the x axis).

A straightforward explanation of this effect is given by the fact that the existence of a debonding length prevents cohesive contacts to be immediately lost when contacts open. In the case of a zero debonding length, the cohesive interaction vanishes as soon as the distance between the two grains mass centre exceeds the sum of their diameter. The cohesive contact is simply lost. By contrast, the existence of a debonding length coincides with a local "virtual" increase of the contacting grains diameters. The cohesive interaction is thus maintained even when the distance between the two grains mass centres exceeds the sum of their diameter. The cohesive contact is preserved, and the stability of the packing increases.
An illustration of this effect is given in Figure 6. The sample corresponding to a contact adhesion B_{og}= 30 (already visible in Figure 1), is shown at instant $t/T = 0.14$, for the different values of the debonding factor $k_{db} = 5.10^{-4}$, 1.10^{-3}, 2.10^{-2} and 1.10^{-1}. The case

$k_{db} = 0$ is also shown for comparision. The stability induced by larger values of k_{db} is betrayed by the lighter gray shade (*i.e.* smaller displacements) of the displaced grains.

4.3 Increasing the density of cohesive contacts

Expectedly, the existence of a debonding length, preserving the existence of cohesive contacts, increases their number. For the three values of the Bond number shown in Figure 7, the mean number of cohesive contacts per particles Z_c as a function of the debonding factor k_{db} is displayed in Figure 8.

A first observation is that the larger the debonding length, the greater the number of cohesive contacts. A second observation is that the case $\ell_{db} = 0$ seems to coincide with a singular behaviour compared to the case $\ell_{db} \neq 0$, at least for the strong contact adhesion. In the case $B_{og} = 60$ for instance, Z_c jumps from 0.86 for $k_{db} = 0$ to $Z_c = 1.16$ (namely an increase of 35%) for a debonding length as small as $\ell_{db}/d = 5.10^{-4}$. Yet increasing further ℓ_{db}/d to a huge 1.10^{-1} increases Z_c to 1.24, namely a mere 7% increase.

It thus seems that the existence of a debonding length, for large values of the contact adhesion, corresponds to a discontinuity of the cohesive packings behaviour. A similar conclusion arises when probing the frictional properties of the samples.

4.4 Increasing the apparent friction

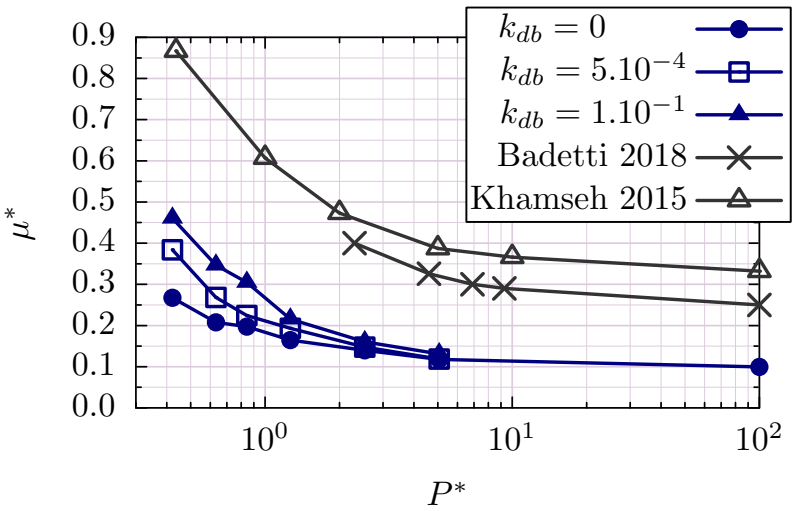

Figure 9: Apparent friction μ^* computed in the failure over the whole simulation as a function of the reduced pressure P^*, for three different debonding factor $k_{db} = \ell_{db}/d$: $k_{db} = 0$, $k_{db} = 5.10^{-4}$ and $k_{db} = 1.10^{-1}$. The data from [5, 6] are also reproduced.

Following the same protocole as in section 3, we estimate the apparent friction μ^* for

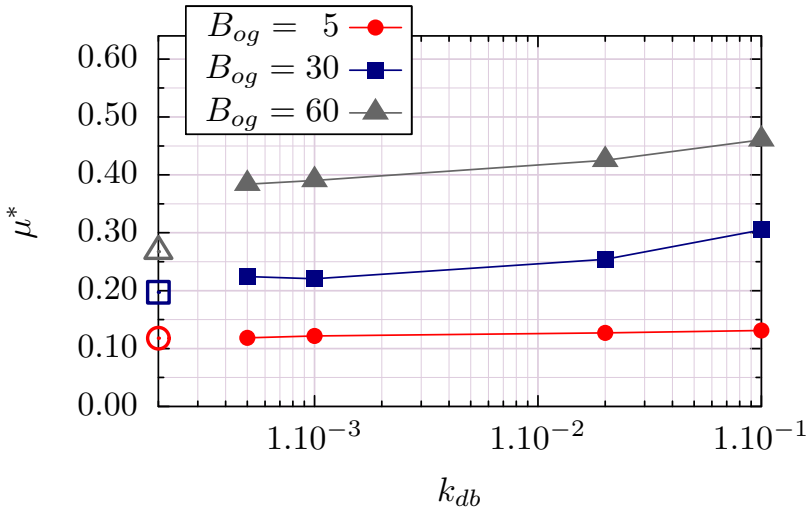

Figure 10: Apparent friction μ^* as a function of the debonding factor k_{db} for three values of the contact adhesion B_{og}. We observe a sharp increase of μ^* between $k_{db} = 0$ (empty symbols) and $k_{db} = 5.10^{-4}$ for a strong contact adhesion (B_{og}= 60).

all values of the granular Bond number B_{og}= 5, 10, 20, 30, 40 and 60, and for all values of the debonding factor $k_{db} = 5.10^{-4}$, 1.10^{-3}, 2.10^{-2} and 1.10^{-1}. The results are displayed in Figure 9 and Figure 10.

Figure 9 shows the apparent friction as a function of the reduced pressure P^* for two different debonding length $\ell_{db}/d = 5.10^{-4}$ and $\ell_{db}/d = 1.10^{-1}$. The case $\ell_{db}/d = 0$ is also shown, together with the data from [5, 6] as in Figure 4. We observe that for both values of $k_{db} = \ell_{db}/d$, the apparent friction is significantly increased; this is particularly true for small values of P^*, namely large values of B_{og}.

Figure 10 shows more particularly the effect of the debonding length on the value of μ^* for three values of the contact adhesion: small (B_{og}= 0), medium (B_{og}= 30) and large (B_{og}=60). We observe how increasing the debonding length increases the apparent friction, specifically for large contact adhesion. We also clearly observe, in the case B_{og}= 60, how the value of the apparent friction jumps when k_{db} goes from 0 to 5.10^{-4}. As is the case for the density of cohesive contacts Z_c displayed in Figure 8, the existence of a non-zero debonding length coincides with a sharp modification of the mean behaviour.

5 EFFECT ON ALGORITHMIC PERFORMANCES

The Contact Dynamics algorithm relies on an implicit formulation of the relation between contact forces and grains velocities. Hence, the resolution implies an iteration loop and a convergence criteria, the latter setting the precision of the algorithm. An easy proxy of the performance of the algorithm may be the mean number of iteration necessary to reach the convergence criteria.
However, in our case, the number of simulations is too sparse to allow for a definite con-

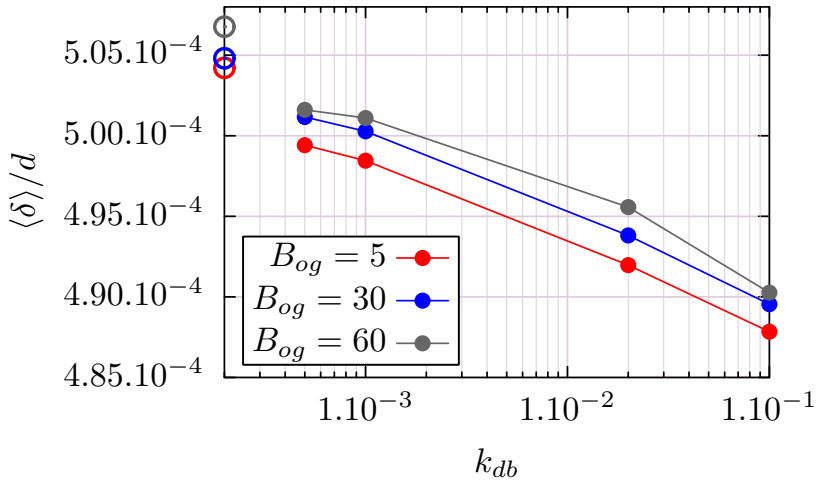

Figure 11: Mean overlap at contacts normalised by the grain diameter δ/d as a function of the debonding factor $k_{db} = \ell_{db}/d$ for three different values of the granular Bond number B_{og}. The cases corresponding to no debonding distance $k_{db} = 0$ are also shown (empty symbols).

clusion: we are considering a single simulation for each (B_{og}, k_{db}) pair. We hence turn to another quatification of the code performance.
The Contact Dynamics algorithm relies on the assumption that the grains are perfectly rigid. Equivalently, two grains involved in a contact do not overlap: the distance between their two centres of mass cannot be smaller than the sum of their radius (in the case of circular grains). In practice however, a contact is detected if an overlap exists; it should however be kept to a minimum value by the resolution loop which, by determining a new set of value for contact forces, imposes a new set of velocities, hence a new set of grains positions. A reliable algorithm will thus keep the mean contacts overlap to a very small value. We chose the mean overlap value, denoted δ in the following, as a quantification of the algorithm performance.
Figure 11 shows the behaviour of δ/d with the debonding factor $k_{db} = \ell_{db}/d$, for three values of the contact adhesion B_{og}= 5, 30 and B_{og}= 60. We first observe how large adhesion coincides with larger values of overlap, although the latter remains small in all cases: $\delta/d \simeq 5.5.10^{-4}$ for $k_{db} = 0$.. We then clearly see how larger debonding lengths induce smaller overlapping at contacts.
Hence, we conclude that the implementation of debonding length in the cohesive contact law does not compromise the precision of the algorithm. Rather, the existence of a debonding length prevents overlap to accumulate at long-lasting cohesive contacts.

6 CONCLUSION

In this contribution, we have explored how the behaviour of a failing cohesive step was dependent on the intensity of the contact adhesion, and on the existence and extent of a debonding length. To this end, 35 independent simulations were carried out applying

a Contact Dynamics algorithm. Because we are interested in the behaviour at incipient failure, the collapsing dynamics was not included in the study.
We first study how contact adhesion strength coincides with stronger pile stability and larger apparent friction in the absence of any debonding length. We then study how the existence of a larger debonding length significantly stabilizes the system, and increases the internal friction, in agreement with both experimental and numerical studies of homogeneous shear flows [5, 6]. At large adhesion strength, we observe the existence of a sharp modification of the behaviour of the system even in the case of a very small debounding length, compared to the case of the absence of the latter.
Finally, we compare the performance of the algorithm in the different cases. We show how increasing the debonding length leads to smaller overlap at contacts, improving the precision of the hard-core hypothesis, fundamental in the algorithm.

REFERENCES

[1] P. Pierrat, D. K. Agrawal, H. S. Caram, Effect of moisture on yield locus of granular materials: theory of shift, PowderTechnology **99**, 220-227 (1998).

[2] Klausner, J. F., Chen, D., & Mei, R., Experimental investigation of cohesive powder rheology, Powder Technology, **112**(1-2), 94-101 (2000)

[3] G. Lumay, F. Boschini, K. Traina, S. Bontempi, J.-C. Remy, R. Cloots, N. Vandewalle, Measuring the flowing properties of powders and grains, Powder Technology **224**, 19-27 (2012).

[4] Richefeu V., M.S. El Youssoufi, F. Radjai, Shear strength properties of wet granular materials, Phys. Rev. E **73** (5), 051304 (2006).

[5] Khamseh, S. , J.-N. Roux, F. Chevoir, Flow of wet granular materials: a numerical study, Phys. Rev. E **92**, 022201 (2015).

[6] M. Badetti, A. Fall, D. Hautemayou, F. Chevoir, P. Aimedieu, S. Rodts, and J.-N. Roux, Rheology and microstructure of unsaturated wet granular materials: Experiments and simulations, J. of Rheology **62**, 1175, doi: 10.1122/1.5026979 (2018)

[7] A. Gans, O. Pouliquen, M. Nicolas, Cohesion-controlled granular material, Phys. Rev. E **101**, 032904 (2020).

[8] S. Deboeuf and A. Fall, Cohesion and aggregates in unsaturated wet granular flows down a rough incline, Journal of Rheology **67** (4), 909-909 (2023)

[9] Rognon P. G., J.-N. Roux, M. Naaïm and F. Chevoir, Dense flows of cohesive granular materials, J. Fluid Mech. vol. **596**, pp. 21–47 (2008).

[10] Mandal, S., M. Nicolas, and O. Pouliquen, Insights into the rheology of cohesive granular media, Proc. Natl. Acad. Sci. U.S.A. **117**, 8366-8373 (2020).

[11] F. Radjai, V. Richefeu, Contact dynamics as a nonsmooth discrete element method, Mech. Mater. **41**, 715-728 (2009)

[12] Nase, S. T., W. L. Vargas, A. A. Abatan, and J. McCarthy, Discrete characterization tools for cohesive granular material, Powder Technol. **116**, 214-223 (2001).

[13] Rumpf, H.C.H., Zur Theorie der Zugfestigkeit von Agglomeraten bei Kraftübertragung an Kontaktpunkten. Chemie Ingenieur Technik, **42**: 538-540 (1970).

[14] L. Staron, L. Duchemin, P.-Y. Lagrée, Cohesive granular columns collapsing: numerics questioning failure, cohesion, and friction, To appear in Journal of Rheology , `https://www.doi.org/10.1122/8.0000674` (2023)

[15] A. Abramian, P.Y. Lagrée, L. Staron, How cohesion controls the roughness of a granular deposit, Soft Matter **17** (47), 10723-10729 (2021).

[16] A. Abramian, L. Staron, P.Y. Lagrée, The slumping of a cohesive granular column: Continuum and discrete modelling, J. Rheol. **64**, 1227-1235 (2020).